Inorganic Chemistry
Article

Inorg. Chem. **2010**, *49*, 10415–10421 **10415**
DOI: 10.1021/ic1018482

Crucial Role of the Reaction Conditions in Isolating Several Metastable Phases in a Gd−Ce−Zr−O System

B. P. Mandal, R. Shukla, S. N. Achary, and A. K. Tyagi*

Chemistry Division, Bhabha Atomic Research Centre, Mumbai 400 085, India

Received June 17, 2010

A series of samples with composition $Gd_{2-y}Ce_yZr_2O_7$ ($0.0 \leq y \leq 2.0$) were prepared by the gel combustion method followed by high-temperature reduction. The details of the structural variations as a function of the composition, temperature, and oxygen stoichiometry have been investigated by X-ray diffraction (XRD), high-temperature XRD (HT-XRD), and thermogravimetry. A complete solubility of Gd^{3+} in $Ce_2Zr_2O_7$ and $Ce_2Zr_2O_8$ could be achieved by this adaptive preparative method. Analysis of the XRD data revealed a sequential variation of the structural features with oxygen stoichiometry as well as Gd^{3+} contents in these compositions. The variation in the unit cell parameter along the compositions has a strong influence on the oxygen uptake behavior in the $Gd_{2-y}Ce_yZr_2O_7$ system, as observed from the thermogravimetric and HT-XRD studies. The preparation and stability of various metastable phases in Gd−Ce−Zr−O have been addressed in detail. The details of the study will be useful for the design and application of a potential redox catalyst and an oxygen storage capacitor.

1. Introduction

Pyrochlore represents a class of materials having the general structural formula $^{VIII}A_2{}^{VI}B_2{}^{IV}X_6{}^{IV}Y$ (Roman numerals indicate the coordination number), where A is a trivalent rare-earth ion or mono- or divalent cation of larger ionic radius and B is a 3d, 4d, or 5d transition element of the appropriate ionic radius and oxidation state. The phase stability of the pyrochlore structure is basically determined by the A and B site cation radius ratio ($r_A/r_B = 1.45-1.80$).[1] However, the radius ratio can be further extended under high-pressure synthetic conditions.[2] It is essential to mention here that a lower radius ratio (i.e., $<\sim 1.45$) favors the formation of an anion-deficient fluorite lattice because of antisite diffusion of the constituent cations. The ordering of cations and anions in a defect fluorite lattice lowers the symmetry from $Fm\bar{3}m$ (fluorite) to $Fd\bar{3}m$ (pyrochlore) with a concurrent doubling of the unit cell parameters. The anion and vacancy ordering plays a significant role in governing the stability and physical properties of pyrochlores under nonambient conditions of temperature and pressure.[3−15] The interesting crystal chemistry originating from cation and anion nonstoichiometry and compositions at different temperatures and pressures has thus been a key interest for structural studies in pyrochlore-type materials. In addition to these structural features, their interesting fundamental and applied properties, like high oxygen mobility,[4,5] oxygen ion sensing,[6] catalytic properties,[7,8] as a host matrix for nuclear waste immobilization,[9,10] and as a host materials for photoluminescence,[11] make them further attractive for contemporary research. In particular, the pyrochlore-type compositions containing zirconium find applications in the fixation of actinides from nuclear wastes[9,10] and as thermal barrier coatings in space crafts and turbines used at elevated temperature.[12]

Further, the cerium-based zirconate pyrochlore $Ce_2Zr_2O_7$ attracts special attention because of the potential catalytic

*To whom correspondence should be addressed. E-mail: aktyagi@barc.gov.in. Phone: 0091-22-25592328. Fax: 0091-22-25505151.

(1) Subramanian, M. A.; Aravamudan, G.; Subba Rao, G. V. *Prog. Solid State Chem.* **1983**, *15*, 55.
(2) Sleight, A. W. *Inorg. Chem.* **1968**, *7*, 1704.
(3) Zhang, F. X.; Wang, J. W.; Lian, J.; Lang, M. K.; Becker, U.; Ewing, R. C. *Phys. Rev. Lett.* **2008**, *100*, 045503.
(4) Mandal, B. P.; Deshpande, S. K.; Tyagi, A. K. *J. Mater. Res.* **2008**, *23*, 911.
(5) Mandal, B. P.; Dutta, A.; Deshpande, S. K.; Basu, R. N.; Tyagi, A. K. *J. Mater. Res.* **2009**, *24*, 2855.
(6) Moon, P. K.; Tuller, H. L. *Sens. Actuators B* **1990**, *1*, 199.
(7) Loong, C. K.; Richardson, J. W.; Ojawa, M. *J. Catal.* **1995**, *157*, 636.
(8) Haynes, D. J.; Berry, D. A.; Shekhawat, D.; Spivey, J. J. *Catal. Today* **2008**, *136*, 206.
(9) Ewing, R. C. *Proc. Natl. Acad. Sci. U.S.A.* **1999**, *96*, 3432.
(10) Ewing, R. C.; Weber, W. J.; Lian, J. *J. Appl. Phys.* **2004**, *95*, 5949.
(11) Nigam, S.; Sudarsan, V.; Vatsa, R. K.; Ghattak, J.; Satyam, P. V. *J. Phys. Chem. C* **2009**, *113*, 8750.
(12) Popa, K.; Konings, R. J. M.; Wastin, F.; Colineau, E.; Magnani, N.; Raison, P. E. *J. Phys. Chem. Solids* **2008**, *68*, 70.
(13) Monte, R.; Kaspar, J. *J. Mater. Chem.* **2005**, *15*, 633.
(14) Fornasiero, P.; Balducci, G.; Kaspar, J.; Meriani, S.; Monte, R.; Graziani, M. *Catal. Today* **1996**, *29*, 47.
(15) Daturi, M.; Finocchio, E.; Binet, C.; Lavalley, J. C.; Fally, F.; Perrichon, V.; Vidal, H.; Hickey, N.; Kaspar, J. *J. Phys. Chem. B* **2000**, *104*, 9186.

Published on Web 10/19/2010

application of the CeO_2-ZrO_2 system in various chemical reactions.[13−20] The ease of oxygen intercalation and deintercalation in CeO_2-based systems makes them promising oxygen storage capacitors. The mechanistic studies revealed that the oxygen stoichiometry arising as a result of varied Ce^{4+} and Ce^{3+} ratios plays an important role in $Ce_2Zr_2O_7$ for oxygen storage and release at relatively lower temperature by fluctuation of the oxidation state of cerium. It has been reported that the efficiency of the redox reactions of the CeO_2-ZrO_2 system depends on the pretreatment like mild or severe oxidation or reduction.[21−23] In various catalytic applications, the lattice structure collapses because of the phase instability during the redox process and, hence, exhibits a diminished performance after a few cycles. Therefore, the systems like pyrochlore, where the lattice remains intact even after repeated redox processes, are preferable. However, the stability of the pyrochlore lattice is mainly governed by the ionic radius of the cations. The crystal chemical properties of the CeO_2-ZrO_2 system studied under different redox conditions indicate that the pyrochlore lattice can be maintained during a mild oxygen intercalation.[24−26] Thus, retention of the pyrochlore lattice with Ce^{4+} under various experimental conditions has been explored in several reports.[27−32] The phase evolution studies in CeO_2-ZrO_2 indicate several stable phases, like most commonly Ce-rich ZrO_2 and Zr-rich CeO_2, in addition to various metastable phases, like κ-$Ce_2Zr_2O_8$ and t and t′ $Ce_2Zr_2O_8$. The instability of the stoichiometric CeO_2-ZrO_2 system with the pyrochlore structure at higher temperatures imposes a major challenge on the synthetic methods. In order to fine-tune the relative stability of the metastable phases by the incorporation of stable trivalent ions like Gd^{3+}, a detailed study on the Ce−Gd−Zr-O system under different preparation conditions is carried out. Several metastable phases have been isolated, for the first time, by adopting various modified reaction parameters. The formation of the phases and their stability under different temperatures and environments are explained in this manuscript.

2. Experimental Details

Analytical reagant grade powders of Gd_2O_3, $ZrO(NO_3)_2 \cdot 5H_2O$, $Ce(NO_3)_3 \cdot 6H_2O$, and glycine were used as the starting reagents. Gd_2O_3 was preheated at 700 °C to remove moisture and other volatile impurities, if any. Subsequently, it was dissolved in a minimum amount of dilute HNO_3. In order to prepare $Gd_{2-y}Ce_yZr_2O_7$ ($0.0 \le y \le 2.0$) compositions, appropriate amounts of metal nitrates were mixed together in demineralized water. Glycine has been added as a fuel in the solution in a stoichiometric ratio. Highly viscous gels were obtained by thermal dehydration (at ≈80 °C) of these solutions. The gels formed upon further heating undergo autoignition with rapid evolution of a large volume of gases to produce voluminous powders. In order to get rid of the excess carbonaceous materials, the powders obtained after autoignition were calcined at 873 K for 45 min. The pellets of the obtained fluffy powders were wrapped in tantalum foil and heated in the presence of zirconium metal (1:5 mole ratio) at 1273 K for 24 h inside an evacuated (10^{-6} Torr) quartz tube.

X-ray diffraction (XRD) patterns of all of the powder samples have been recorded on a Panalytical X'pert Pro XRD unit using Cu Kα radiation. For study of the thermal stability of the compositions in the series, the XRD patterns were recorded between 293 and 1273 K at a regular interval of 200 K on a Philips X'pert Pro XRD unit equipped with an Anton Paar HTK attachment. Thermogravimetric (TG) studies were carried out using a Netzsch 409 PC LUXX instrument in the range 293−1273 K in dynamic air. The samples were filled in an alumina crucible for this experiment, and the flow of air was 110 mL/min in TG measurements. The Raman spectra were recorded using an indigenously developed micro-Raman system. In this instrument, a 20× objective is used with confocal optics and a CCD-based single-stage spectrograph along with a supernotch filter. A solid-state diode laser with a 532 nm line was used as the excitation source. The compositional characterizations of these samples were carried out using a JEOL JSM840 microscope attached with a EDS facility.

3. Results and Discussion

The typical powder XRD patterns of the samples obtained after calcination at 873 K are depicted in Figure 1a. The XRD patterns of all the samples do not indicate any segregated secondary phases, like Gd_2O_3, CeO_2, and ZrO_2 etc. Thus the composition of the products obtained after combustion process can be generalized as $Gd_{2-y}Ce_yZr_2O_{7+\delta}$ considering the possible aerial oxidation of Ce^{3+} ions to Ce^{4+}.[24,25] The elemental ratio of Gd: Ce: Zr in different compositions as per EDS data are summarized in Table 1. The powder XRD patterns of all the compositions show characteristic reflections of fluorite-type lattice but with appreciable broadening. The broadening of the reflections can be attributed to the nano nature of these samples. The average crystallite sizes estimated by Scherrer formula were found to be in the range of 5−7 nm in these compositions. It is important to note here that all the Gd^{3+} containing compositions show significantly larger broadening compared to the $Ce_2Zr_2O_{7+\delta}$, though these samples are prepared under identical conditions. Such feature can be resulted from the difference in sinterability or inherent local distortion in the samples.

The formation of a pyrochlore-type ordered lattice can be inferred from the superstructure reflection (at $2\theta \sim 27.6°$,

(16) Mandal, B. P.; Grover, V.; Pai, M. R.; Tyagi, A. K. *J. Mater. Res.* **2009**, *24*, 2845.
(17) Campbell, C. T.; Peden, C. H. F. *Science* **2005**, *309*, 713.
(18) Vlaic, G.; Fornasiero, P.; Geremia, S.; Kaspar, J.; Graziani, M. *J. Catal.* **1997**, *168*, 386.
(19) Bernal, S.; Blanco, G.; Calvino, J. J.; Hernandez, J. C.; Perez-Omil, J. A.; Pintado, J. M.; Yeste, M. P. *J. Alloys Compd.* **2008**, *451*, 521.
(20) Montini, T.; Baares, M. A.; Hickey, N.; Di Monte, R.; Fornasiero, P.; Kaspar, J.; Graziani, M. *Phys. Chem. Chem. Phys.* **2004**, *6*, 1.
(21) Fornasiero, P.; Fonda, E.; Di Monte, R.; Vlaic, G.; Kaspar, J.; Graziani, M. *J. Catal.* **1999**, *187*, 177.
(22) Fornasiero, P.; Montini, T.; Graziani, M.; Kaspar, J.; Hungn, A. B.; Martiez-Arias, A.; Conesa, J. C. *Phys. Chem. Chem. Phys.* **2002**, *4*, 149.
(23) Kaspar, J.; Di Monte, R.; Fornasiero, P.; Graziani, M.; Bradshaw, H.; Norman, C. *Top. Catal.* **2001**, *16−17*, 83.
(24) Achary, S. N.; Sali, S. K.; Kulkarni, N. K.; Krishna, P. S. R.; Shinde, A. B.; Tyagi, A. K. *Chem. Mater.* **2009**, *21*, 5848.
(25) Kishimoto, H.; Takahisa, O.; Otsuka-Yao-Matsuo, S.; Ueda, K.; Hosono, H.; Kawazoe, H. *J. Alloys Compd.* **2000**, *312*, 94.
(26) Thomson, J. B.; Armstrong, A. R.; Bruce, P. G. *J. Solid State Chem.* **1999**, *148*, 56.
(27) Patwe, S. J.; Ambekar, B. R.; Tyagi, A. K. *J. Alloys Compd.* **2005**, *389*, 243.
(28) Varez, A.; Garcia-Gonzalez, E.; Sanz, J. *J. Mater. Chem.* **2006**, *16*, 4249.
(29) Yashima, M.; Arashi, H.; Kakihana, M.; Yoshimura, M. *J. Am. Ceram. Soc.* **1994**, *77*, 1067.
(30) Yashima, M.; Sasaki, S.; Kakihana, M.; Yamaguchi, Y.; Arashi, H.; Yoshimura, M. *Acta Crystallogr., Sect. B* **1994**, *50*, 663.
(31) Omata, T.; Kishimoto, H.; Otsuka-Yao-Matsuo, S.; Ohtori, N.; Umesaki, N. *J. Solid State Chem.* **1999**, *147*, 573.
(32) Otsuka-Yao-Matsuo, S.; Omata, T.; Izu, N.; Kishimoto, H. *J. Solid State Chem.* **1998**, *138*, 47.

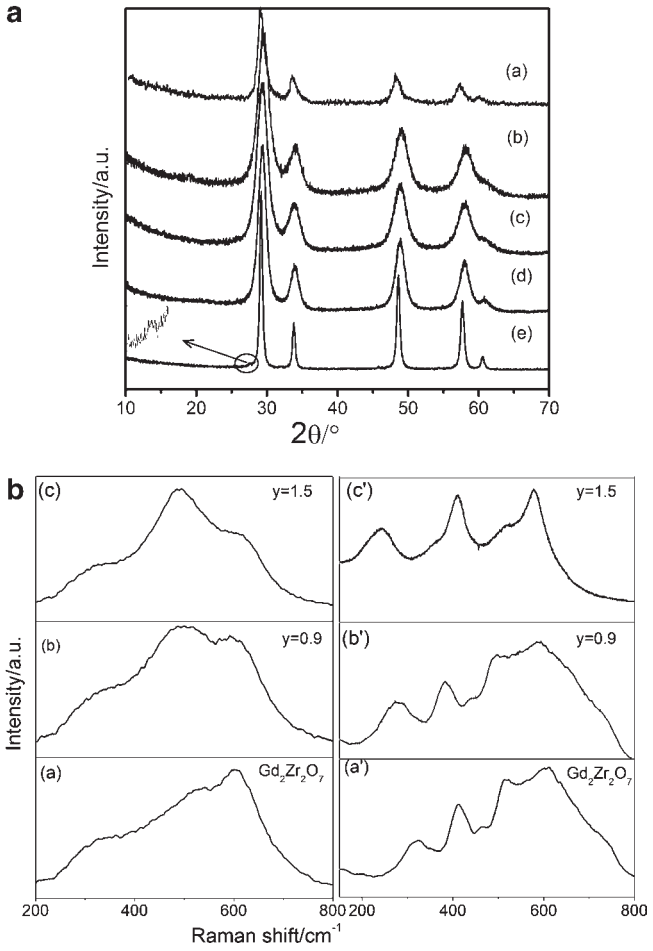

Figure 1. (a) XRD patterns of as-prepared samples of the $Gd_{2-y}Ce_yZr_2O_{7+\delta}$ series: (a) $Gd_2Zr_2O_7$; (b) $Gd_{1.4}Ce_{0.6}Zr_2O_{7.3}$; (c) $Gd_{1.1}Ce_{0.9}Zr_2O_{7.45}$; (d) $Gd_{0.5}Ce_{1.5}Zr_2O_{7.75}$; (e) $Ce_2Zr_2O_8$. Inset: superstructure peak of $Ce_2Zr_2O_8$. (b) Raman spectra of as-prepared (a) $Gd_2Zr_2O_7$, (b) $Gd_{1.1}Ce_{0.9}Zr_2O_{7+\delta}$, and (c) $Gd_{0.5}Ce_{1.5}Zr_2O_{7+\delta}$ and sintered (a′) $Gd_2Zr_2O_7$, (b′) $Gd_{1.1}Ce_{0.9}Zr_2O_7$, and (d) $Gd_{0.5}Ce_{1.5}Zr_2O_7$.

Table 1. Elemental Ratio (atom %) in $Gd_{2-y}Ce_yZr_2O_7$ Compositions as per the EDS Data

	Gd	Ce	Zr
$Gd_2Zr_2O_7$	2.01(3)		2.02(2)
$Gd_{1.7}Ce_{0.3}Zr_2O_7$	1.68(2)	0.30(4)	1.98(3)
$Gd_{1.4}Ce_{0.6}Zr_2O_7$	1.39(3)	0.61(4)	2.01(3)
$Gd_{1.1}Ce_{0.9}Zr_2O_7$	1.11(2)	0.91(3)	2.01(3)
$Gd_{0.8}Ce_{1.2}Zr_2O_7$	0.81(2)	1.21(4)	2.01(2)
$Gd_{0.5}Ce_{1.5}Zr_2O_7$	0.50(3)	1.49(2)	1.98(2)
$Ce_2Zr_2O_7$		2.01(2)	1.99(3)

indicated in Figure 1a) from the XRD pattern of the composition with Ce:Zr in 1:1 mole ratio, even though the ionic radii of Ce^{4+} (0.97 Å in 8-fold coordination) and Zr^{4+} (0.72 Å in 6-fold coordination) are closer to each other compared to Gd^{3+} (1.05 Å in 8-fold coordination) and Zr^{4+}.[33] The Ce:Zr = 1:1 stoichiometric composition can be related to the cubic $Ce_2Zr_2O_8$ or cation-ordered $Ce_2Zr_2O_{7+\delta}$ phase as reported in the literature.[24−26] Thus, it can be inferred that the formation of $Ce_2Zr_2O_{7+\delta}$ might be following the path of formation of a cation-ordered pyrochlore lattice, $Ce_2Zr_2O_7$, followed by its oxidation to a $Ce_2Zr_2O_{7+\delta}$-type lattice. Retention of a cation-ordered lattice in the oxidation from $Ce_2Zr_2O_7$ to $Ce_2Zr_2O_8$ has been explained in several reports.[24−26] On the other hand, the Gd^{3+}-rich compositions might be leading to a cation-disordered fluorite lattice, because of the relatively smaller ionic radius difference between Gd^{3+} and Zr^{4+} ions. The predominant cation ordering in $Ce_2Zr_2O_{7+\delta}$ samples might be related to the larger differences in the cationic radius of the Ce^{3+} (1.14 Å in 8-fold coordination) and Zr^{4+} ions compared to that of the Gd^{3+} and Zr^{4+} ions.

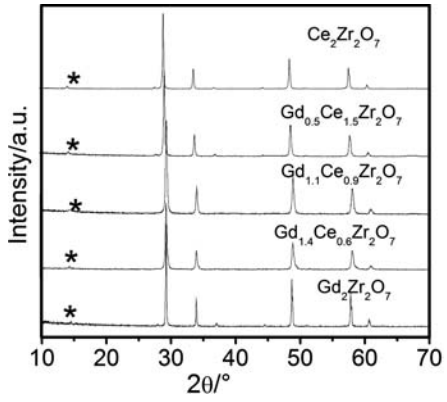

Figure 2. Typical XRD patterns of the $Gd_{2-y}Ce_yZr_2O_7$ pyrochlore series (asterisks correspond to the superstructure peaks).

Further insights about the structural and cation-ordering features of these compositions have been drawn from Raman spectroscopic studies. Raman spectroscopy is primarily sensitive to oxygen-cation vibrations and is an excellent probe for local disorder. Often Raman spectroscopic investigations provide unequivocal information to differentiate closely related structures, as is the case in the present study. It has been extensively used to distinguish disordered pyrochlore and defect fluorite materials, where the structural difference arises from the local disorder around the A or B cations.[34] Therefore, Raman spectroscopy has been performed on the as-prepared and reduced samples to examine the presence (leading to the pyrochlore structure) or absence (leading to the defect fluorite structure) of ordering in the samples. The Raman spectra of some representative as-prepared and corresponding reduced compositions are shown Figure 1b. It has been found that the peaks are very broad for the as-prepared samples and display features similar to those reported earlier for defect fluorite materials.[34−37] The Raman spectra of sintered $Gd_2Zr_2O_7$, $Gd_{1.1}Ce_{0.9}Zr_2O_7$, and $Gd_{0.5}Ce_{1.5}Zr_2O_7$ (reduced at 1273 K) are distinct and well-defined, which indicates that these compositions adopt the pyrochlore structure.

The further detailed structural features of these samples were studied after heating them at low oxygen partial pressure. The low oxygen partial pressure ($\sim 10^{-20}$ atm) provided by Zr(s)−O_2(g) equilibrium causes the reduction of Ce^{4+} to Ce^{3+} in all cerium containing compositions.[38] Thus, the

(33) Shannon, R. D. *Acta Crystallogr.* **1976**, *A32*, 751.
(34) Glerup, M.; Nielsen, O. F.; Poulsen, F. W. *J. Solid State Chem.* **2001**, *160*, 25.
(35) Mandal, B. P.; Krishna, P. S. R.; Tyagi, A. K. *J. Solid State Chem.* **2010**, *183*, 41.
(36) Mandal, B. P.; Garg, N.; Sharma, S. M.; Tyagi, A. K. *J. Solid State Chem.* **2006**, *179*, 1999.
(37) Xia, X.; Ouyang, J.; Liu, Z. *J. Am. Ceram. Soc.* **2010**, *93*, 1074.
(38) Ackeramnn, R. J.; Chandrasekharaiah, M. S. *Systematic Thermodynamic Properties of Actindes Metal Oxygen Systems at High Temperature, Emphasis on Lower Valence States, Thermodynamics of Nuclear Materials*; IAEA: Vienna, Austria, 1975; Vol. *II*, pp 3−26.

Table 2. Lattice Parameters (Å) of $Gd_{2-y}Ce_yZr_2O_7$ at Different Temperatures (K)

	temperature (K)						
composition	RT	473	673	873	1073	1273	RTC[a]
$Gd_2Zr_2O_7$	10.501(1)	10.520(1)	10.569(2)	10.570(2)	10.616(1)	10.644(1)	10.501(1)
$Gd_{1.7}Ce_{0.3}Zr_2O_7$	10.508 (1)	10.521(2)	10.574(1)	10.584(1)	10.624(2)	10.646(1)	10.508(2)
$Gd_{1.4}Ce_{0.6}Zr_2O_7$	10.512(2)	10.522(1)	10.540(1)	10.573(2)	10.599(1)	10.611(2)	10.510(2)
$Gd_{1.1}Ce_{0.9}Zr_2O_7$	10.523(1)	10.524(2)	10.544(2)	10.571(2)	10.596(2)	10.618(2)	10.520(2)
$Gd_{0.8}Ce_{1.2}Zr_2O_7$	10.527(2)	10.528(2)	10.559(1)	10.580(2)	10.607(1)	10.636(1)	10.522(1)
$Gd_{0.5}Ce_{1.5}Zr_2O_7$	10.565(1)	10.538(2)	10.565(2)	10.593(2)	10.612(2)	10.639(2)	10.529(1)
$Gd_{0.2}Ce_{1.8}Zr_2O_7$	10.625(2)	10.578(1)	10.562(2)	10.589(1)	10.625(2)	10.680(1)	10.542(1)
$Ce_2Zr_2O_7$	10.631(1)	10.578(1)	10.569(1)	10.594(1)	10.631(2)	10.679(2)	10.547(1)

[a] Room temperature cooled.

reduction of Ce^{4+} to Ce^{3+}, leading to an ideal $Gd_{2-y}Ce_yZr_2O_7$ pyrochlore composition, as is evident from the XRD studies. A few representative powder XRD patterns of the samples obtained after this reductive treatment are shown in Figure 2. The appearance of a weak superstructure peak (marked in Figure 2) clearly indicates the formation of a crystalline pyrochlore ($Fd\bar{3}m$) phase in all of the compositions throughout the homogeneity range. In addition, a systematic shift of the diffraction peak positions toward lower angle indicates an increasing trend in the unit cell parameters with increasing cerium concentration in $Gd_{2-y}Ce_yZr_2O_7$ compositions. The unit cell parameters for these compositions were calculated by least-squares refinement and are given in Table 2. The increasing trend of the unit cell parameters with increasing cerium content in the series is in accordance with the ionic radii of Gd^{3+} and Ce^{3+}. It is interesting to note here that the relative intensity of the characteristic superstructure peaks of the pyrochlore lattice systematically increases on going from $Gd_2Zr_2O_7$ to $Ce_2Zr_2O_7$ in this series. The mechanism of the pyrochlore-to-fluorite transition is attributed to an antisite cationic disorder, which is favored by a lower r_A/r_B ratio. Thus, the larger the difference between the A and B site cations, the higher is the degree of order. Therefore, the intensity of the superstructure peaks (degree of order) increases with an increase in the Ce^{3+} content. It is important to mention here that the adopted method of preparation could yield the complete solid solution formation between $Gd_2Zr_2O_7$ and $Ce_2Zr_2O_7$, which has an important role in incorporating Ce^{4+} in the pyrochlore lattice, as explained subsequently.

A complete series of anion-rich pyrochlore phases as $Gd_{2-y}Ce_yZr_2O_{7+\delta}$ was prepared by oxidation of the $Gd_{2-y}Ce_yZr_2O_7$ phases on a thermogravimetry setup. The oxidation process in the solid solution $Gd_{2-y}Ce_yZr_2O_7$ was also measured quantitatively. All of the compositions except $Gd_2Zr_2O_7$ show weight gain due to the oxidation of Ce^{3+} to Ce^{4+}. TG traces for some representative compositions are shown in Figure 3a. It could be inferred from the weight gain that the complete oxidation of Ce^{3+} to Ce^{4+} and thus the final oxygen stoichiometry is related to the cerium content in the compositions. Such an oxidation could lead to a complete substitution of Gd^{3+} by Ce^{4+}, which cannot be achieved by a conventional solid-state reaction. Earlier, only a very small quantity of Ce^{4+} (5 mol %) could be incorporated in the $Gd_2Zr_2O_7$ lattice by a solid-state method.[27] The remarkable success of this new method can be attributed to the gentle deintercalation of oxygen ions from $Gd_{2-y}Ce_yZr_2O_{7+\delta}$, which leads to a $Gd_{2-y}Ce_yZr_2O_7$ pyrochlore lattice in the whole series, i.e., for $0.0 \le y \le 2.0$.

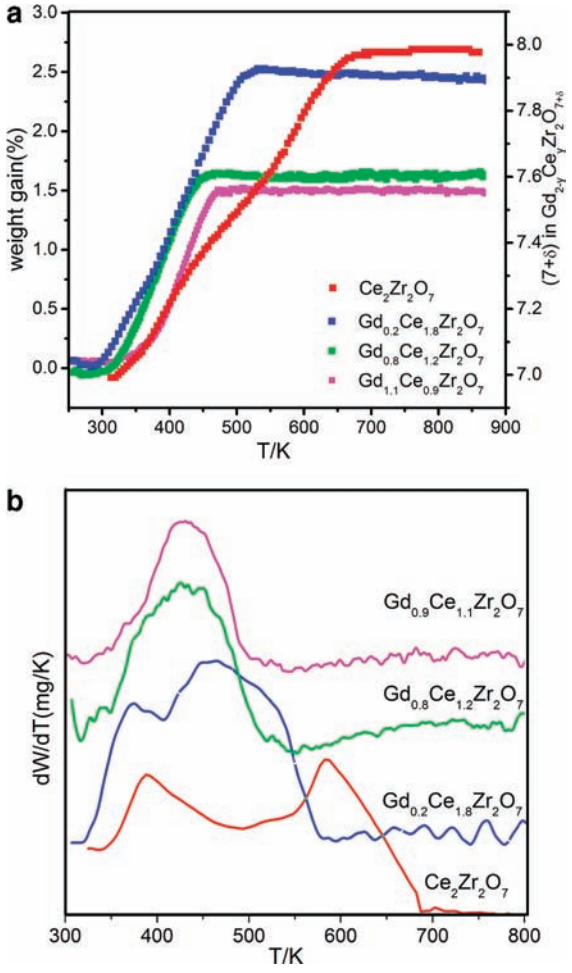

Figure 3. (a) TG of different compositions in $Gd_{2-y}Ce_yZr_2O_7$ systems (the right-side y axis indicates the oxygen content after oxidation). (b) DTG of different compositions in $Gd_{2-y}Ce_yZr_2O_7$ systems.

The total oxidation of the $Gd_{2-y}Ce_yZr_2O_7$ samples occurs in two steps in Ce-rich compositions but in a continuous single step in Gd-rich compositions (Figure 3a). The difference in the oxidation behavior of the samples can be clearly observed from the differential thermogravimetric (DTG) curves. DTG traces for some representative compositions are shown in Figure 3b. The DTG curves of the compositions corresponding to $y = 2$ and 1.8 show two distinct peaks, which are similar to that reported earlier for $Ce_2Zr_2O_7$.[24] The difference between the temperatures of two oxidation steps narrows with a decrease in the cerium content and eventually merges to a single-step oxidation in Gd^{3+}-rich compositions.

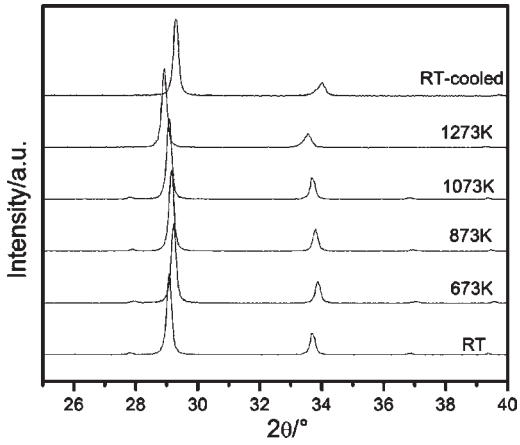

Figure 4. XRD patterns of $Ce_2Zr_2O_7$ at different temperatures up to 1273 K.

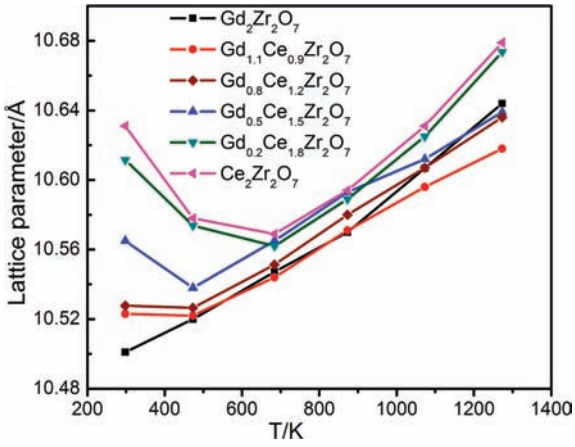

Figure 5. Plot of lattice parameters of different composition as a function of the temperature.

The compositions corresponding to $y = 1.2$ show a broad peak in DTG that might be a summation of two closely spaced peaks. However, the single peak in the DTG of the sample corresponding to $y = 0.9$ clearly implies a single-step oxidation process. Earlier structural studies on the $Ce_2Zr_2O_7$ sample revealed that at relatively lower temperature half of Ce^{3+} oxidizes to give a composition $Ce_2Zr_2O_{7.5}$, and later the rest of Ce^{3+} oxidizes to give a $Ce_2Zr_2O_8$ composition.[24] In all of these three compositions, i.e., $Ce_2Zr_2O_7$, $Ce_2Zr_2O_{7.5}$, and $Ce_2Zr_2O_8$, the cation ordering is retained. In the present study, we observed that the oxidation temperature gradually increases with increasing Gd^{3+} content. This is reflected in a shift of the DTG peak toward higher temperature with increasing Gd^{3+} content. The unit cell contraction in the oxidation process can be attributed to the predominant effect of decreasing ionic radii due to oxidation of Ce^{3+} to Ce^{4+} compared to the incorporation of oxygen in the lattice. In general, contribution of the anion incorporation and the decrease in cation radii play opposite roles on the unit cell parameters. The stability of $Ce_2Zr_2O_{7.5}$ in the oxidation process indicates that a relatively higher temperature is required to oxidize the remaining Ce^{3+}.[24] From the oxidation trend of $Ce_2Zr_2O_7$ and the stability of the $Ce_2Zr_2O_{7.5}$ lattice, it can be inferred that the decrease in the unit cell parameters hinders further intercalation of oxygen in the $Ce_2Zr_2O_{7.5}$ lattice. For this reason, it can be emphasized that the observed increasing trend in the oxidation temperature with an increase in the Gd^{3+} content is related to the channel dimension for oxygen intercalation in the pyrochlore lattice and, hence, to the overall unit cell parameters. In addition, the absence of any intermediate phase in the Gd^{3+}-rich compositions may be attributed to the higher temperature oxidation phenomenon, where a kinetically faster oxygen migration can be expected. Further insight into this unit cell parameter related oxidation behavior is obtained from high-temperature XRD (HT-XRD) studies, which will be explained subsequently.

In order to understand the variation of the cell parameter with oxidation, in situ HT-XRD studies were carried out. The typical HT-XRD patterns of the $Ce_2Zr_2O_7$ sample at various temperatures are shown in Figure 4. The unit cell parameters of different compositions as a function of the temperature are shown in Figure 5. The unit cell parameters of $Gd_{2-y}Ce_yZr_2O_7$, for $y = 0.0-1.2$, show an increasing trend with increasing temperature. However, the unit cell parameters of composition corresponding to $y = 1.5$ show a decreasing trend up to 473 K and then increase linearly. Similarly, the unit cell parameters of the heavily cerium-substituted samples (i.e., $y = 1.8$ and 2.0) show a decreasing trend up to 673 K, followed by an increasing trend with temperature. From Table 2 and Figure 5, three distinct trends in the variation of the unit cell parameters with temperature can be seen. In general, two phenomena, viz., oxidation of Ce^{3+} in cerium-substituted pyrochlores and thermal expansion of the unit cell, take place simultaneously as the samples are heated in air. Thus, the unit cell parameters are controlled by three main factors, like (a) shrinkage of the lattice parameter due to decreases in the ionic radii by the aerial oxidation of Ce^{3+} to Ce^{4+}, (b) expansion of the lattice due to incorporation of extra oxygen in the lattice, and (c) thermal expansion of the lattice due to temperature effects. Earlier studies showed that the effect of oxygen incorporation has an insignificant influence compared to the contribution arising from ionic radii variation.[24] This is further confirmed from the lower values of the unit cell parameters observed for the fully oxidized samples obtained after cooling from 1273 K (Table 2). Thus, it can be mentioned here that the unit cell expansion due to temperature and ionic radii variation is the main controlling factor for the oxygen intercalation process of the pyrochlore system. The linearly increasing unit cell parameter of $Gd_2Zr_2O_7$ throughout the temperature range can be attributed solely to the lattice expansion contribution because neither aerial-oxidation-induced lattice shrinkage nor excess-oxygen-induced expansion is expected in this composition. However, the initial decreasing trend in the unit cell parameter of the Ce-rich compositions in $Gd_{2-y}Ce_yZr_2O_7$, i.e., for $y \geq 1.5$, with increasing temperature is due to the dominating contribution from the oxidation-induced decrease of average ionic radii compared to the contribution of temperature-induced lattice expansion. The increasing trend of the unit cell parameter at higher temperature can be attributed to the predominant thermal affect compared to the oxidation affect.

When the thermal expansion and TG data of all of the $Gd_{2-y}Ce_yZr_2O_7$ compositions are compared, the effect and mode of oxygen incorporation could be delineated. As observed from variation of the unit cell parameters with temperature, we can infer that the lattice dilation provides an

easy oxygen migration path compared to the original lattice of smaller unit cell parameters. Thus, the decrease in the unit cell parameter due to the ionic size effect leads to a minimum volume lattice, where further oxygen incorporation is hindered unless the temperature can induce sufficient expansion and alter the kinetics to fully oxidize them in Ce^{3+}-rich compositions. Therefore, the oxidation behavior of Ce-rich compositions occurs in two steps, as observed in their TG and DTG traces (Figure 3a,b). Another important observation of increasing oxidation temperature with increasing Gd^{3+} content can be explained on the basis of the similar argument of a decreasing trend of the unit cell parameters. It can be mentioned here that the cation ordering of the $Gd_{2-y}Ce_yZr_2O_7$ structure is retained during oxidation of $Gd_{2-y}Ce_yZr_2O_7$ to $Gd_{2-y}Ce_yZr_2O_{7+\delta}$ compositions. The oxidation of Ce^{3+} to Ce^{4+} intercalates extra oxygen atoms to fill the vacant sites of the pyrochlore lattice.[24] Thus, the oxidation process follows a lower activation energy path and, hence, all compositions show weight gain at lower temperature (~325 K). Single-step oxidation at relatively higher temperature in Gd^{3+}-rich compositions suggests that the lower channel size due to smaller unit cell parameters hinders the oxygen migration until the lattice is sufficiently dilated. Because all of the Gd^{3+}-rich compositions show a continuous expansion of the unit cell, no such barrier is imposed for oxidation of Ce^{3+} and, hence, all of the Ce^{3+} ions oxidize in a continuous manner, which is reflected as a single oxidation step in DTG.

Further we have also investigated the thermal and structural stabilities of these compositions at higher temperature after heating at 1673 K in static air for 24 h. The thermal stability of the CeO_2-ZrO_2 system has been studied in several reports.[24,28−32] In these studies, the fully oxidized CeO_2-ZrO_2 composition ($Ce_2Zr_2O_8$) has been reported as tetragonally distorted metastable phases or as a mixture of two fluorite lattices (Ce- and Zr-rich), tetragonal and fluorite, tetragonal, and another tetragonal phase. The formation of a pyrochlore-type $Ce_2Zr_2O_8$ composition is observed only through low-temperature oxidation of $Ce_2Zr_2O_7$. Similar studies on $Gd_2Zr_2O_7$ show a reversible pyrochlore-to-fluorite structural transformation at higher temperature.[39] The difference in the stability and high-temperature behavior of the two end members reflects interestingly in the $Gd_{2-y}Ce_yZr_2O_{7+\delta}$ system. The powder XRD patterns recorded after cooling of the samples from 1673 K to ambient temperature show that the stability and structures of the phases are strongly dependent on the concentration of Gd^{3+}. The XRD patterns of the samples after heating at 1673 K and cooling to room temperature are shown in Figure 6. The initial compositions, viz., $y = 0.0-0.6$, remain as pyrochlore after this heat treatment. The superstructure peak at $2\theta = 14.6°$ is observable as shown in the inset of Figure 6. On the other hand, the compositions corresponding to $y = 0.9-1.5$ undergo a phase transformation to the fluorite lattice. The other compositions, i.e., $y = 1.8$ and 2.0, undergo spinodal decomposition into cubic ceria-rich and tetragonal zirconia-rich phases.

The synthesis method plays an important role in the stabilization of the fluorite-type phases $Gd_{2-y}Ce_yZr_2O_{7+\delta}$ (except $y = 2.0$). The metastable nature of these as-prepared fluorite-type materials (Box-I in Figure 7) can primarily be

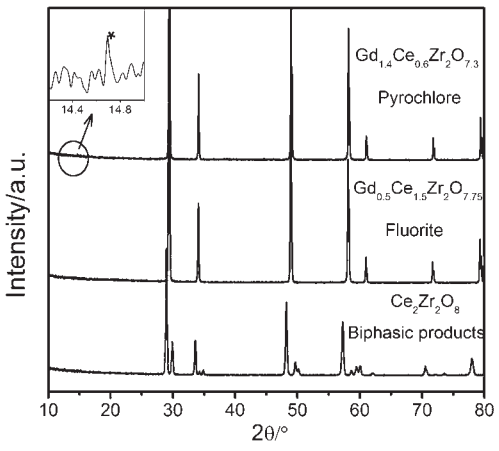

Figure 6. XRD patterns of $Gd_{2-y}Ce_yZr_2O_{7+\delta}$ after heating of the samples at 1400 °C in air. Inset: superstructure peak of $Gd_{1.4}Ce_{0.6}Zr_2O_{7.3}$ at $2\theta = 14.7°$.

attributed to the nanonature of these samples. The present adopted autoignition process gives a high temperature (~1700 K) for shorter duration, where nonequilibrium thermodynamically metastable phases can be stabilized.[40] In addition, such methods of synthesis produce nanocrystalline materials with high surface energy and a relaxed lattice where metastable modification can be stabilized. Thus, the fluorite-type solid solution in the complete series obtained after the combustion reaction can be solely attributed to the nanonature. However, in the case of the composition with $y = 2.0$, the metastable O-rich pyrochlore lattice can be explained by two reaction steps, viz., formation of $Ce_2Zr_2O_7$ from cerium(III) and zirconium(IV) nitrates during combustion and subsequent oxygen intercalation to oxidize Ce^{III} to Ce^{IV}. This is a plausible reason for failure of the conventional solid-state method to prepare $Ce_2Zr_2O_8$.

The $Gd_{2-y}Ce_yZr_2O_7$ pyrochlore-type solid solutions (Box-II in Figure 7), obtained after reduction, are also metastable in nature as they get oxidized to O-rich phases, because of their poor stability in air. The formation of these compositions can be explained by the crystallographic prerequisite (r_A/r_B ratio) for the pyrochlore frame. The transformation of $Gd_{2-y}Ce_yZr_2O_7$ to $Gd_{2-y}Ce_yZr_2O_{7+\delta}$ is a reversible process, which is governed by the temperature and oxygen partial pressure.

The anion-rich phases (Box-III in Figure 7), obtained after oxidation of $Gd_{2-y}Ce_yZr_2O_7$ pyrochlores at 1273 K, are also thermodynamically metastable (from $y = 0.9$ to 2.0). The nature of the transformed phases depends strongly on the cerium content in the $Gd_{2-y}Ce_yZr_2O_{7+\delta}$ composition, as mentioned earlier. The first three compositions (up to $y = 0.0-0.6$) form pyrochlore lattices and are stable up to 1673 K. The compositions corresponding to $y = 0.9-1.5$ transformed to a disordered fluorite-type structure after the heat treatment at 1673 K, which is due to disordering of the cations and anions at that temperature. The compositions corresponding to $y = 1.8-2.0$ undergo a spinodal decomposition into two thermodynamically stable fluorite-type phases. This phase evolution from the samples in Box-III is similar to that of the as-prepared metastable fluorite-type solid solution (Box-I) at high temperature.

(39) Perez, H.; Jorba, Y. *Ann. Chim.* **1962**, *7*, 479.

(40) Mukherjee, S. T.; Bedekar, V.; Patra, A.; Sastry, P. U.; Tyagi, A. K. *J. Alloys Compd.* **2008**, *466*, 493.

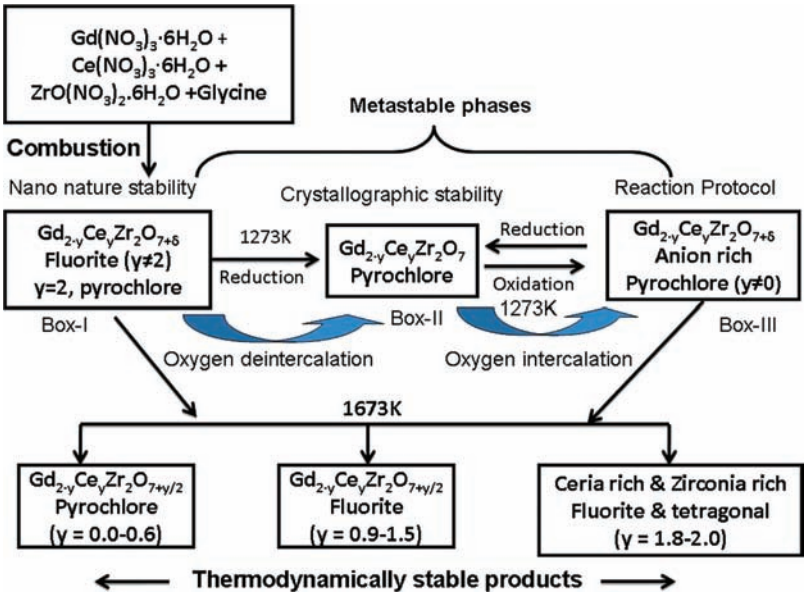

Figure 7. Schematic representation of different phases under different conditions in the $Gd_{2-y}Ce_yZr_2O_7$ system.

In summary, the phase evolution of $Gd_{2-y}Ce_yZr_2O_7$ is strongly controlled by the oxygen stoichiometry, Gd/Ce ratio, and temperature. A schematic representation of different phases under different conditions in the $Gd_{2-y}Ce_yZr_2O_7$ system is shown in Figure 7. The combustion-prepared powders showed fluorite-phase formation except for $Ce_2Zr_2O_{7+\delta}$, which has a cation-ordered lattice. These powders upon reduction in the presence of zirconium sponge formed stable pyrochlore phases with composition $Gd_{2-y}Ce_yZr_2O_7$ ($0.0 \leq y \leq 2.0$). Upon oxidation at relatively lower temperature, all of the compositions form an anion-rich pyrochlore-type lattice similar to the cation-ordered $Ce_2Zr_2O_8$ lattice. Interestingly, oxidation at higher temperature (1673 K) leads to phases governed by the Gd/Ce ratio, which is invariably related to the average r_A/r_B ratio.

4. Conclusions

A unique two-step synthesis method has been developed for the synthesis of Gd^{3+}-substituted $Ce_2Zr_2O_7$ samples. The appropriate reaction conditions for isolating various metastable solid-state solution regions have been established from a systematic study at various temperatures and atmospheres. The phase analysis of the compositions heated at higher temperature (1673 K) revealed that the pyrochlore phase is maintained in Gd-rich samples (i.e., up to $y = 0.6$), while a composition with $0.9 \leq y \leq 1.5$ transforms to the fluorite-type phase. The compositions with $y = 1.8$ and 2.0 undergo spinodal decomposition to cubic ceria-rich and tetragonal zirconia-rich phases. The stability of the compositions at higher temperature is governed by the average ionic radius of Gd^{3+}/Ce^{4+} in $Gd_{2-y}Ce_yZr_2O_{7+\delta}$. The oxidation behavior and stability of the samples could be related to the temperature evolution of the unit cell parameters.

Acknowledgment. The authors acknowledge Dr. N. Raje, ACD, BARC, and Dr. A. Mishra, HP&SRPD, BARC, for fruitful discussions on thermogravimetry and Raman spectroscopic analysis.